

Supplementary Information

Secondary porosity generation in sandstones constrained by the fault movement, fluid flow and mudstone/sandstone interactions, offshore Bohai Bay Basin, China

Huan Li^{a,b}, Xiaofeng Du^b, Xianghua Yang^c, Hongtao Zhu^c

a, School of Geography, Earth and Atmospheric Sciences, University of Melbourne, Victoria 3010, Australia

b, China National Offshore Oil Corporation Limited, Tianjin Branch, Tianjin 300459, China

c, Faculty of Earth Resources, China University of Geosciences, Wuhan 430074, China

1. The example of trap morphologies at CFD1

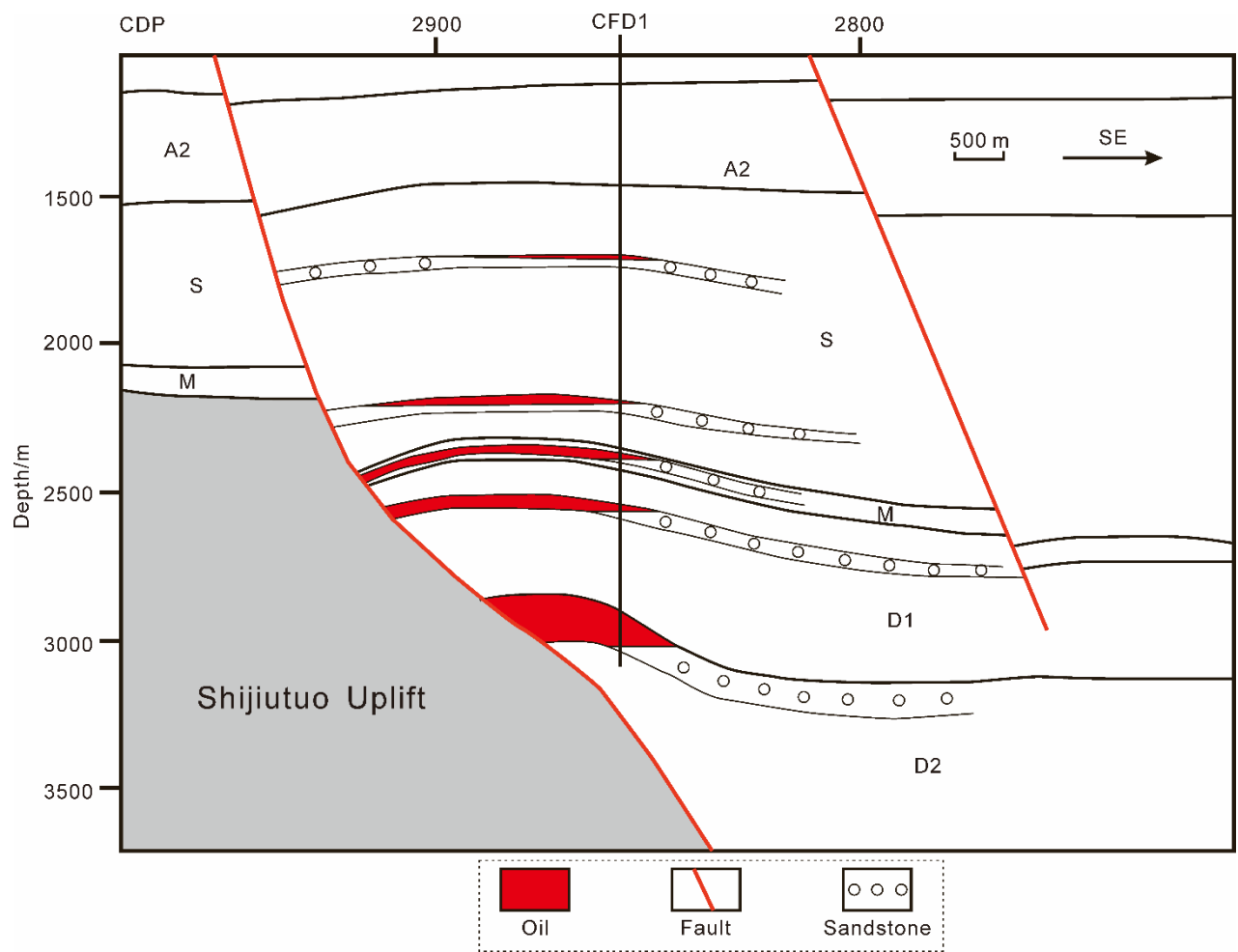


Figure S1. Example of trap morphologies at CFD1 (borehole location is shown in Figure 1B).

2. Lithology, logging, fluid type and sample locations

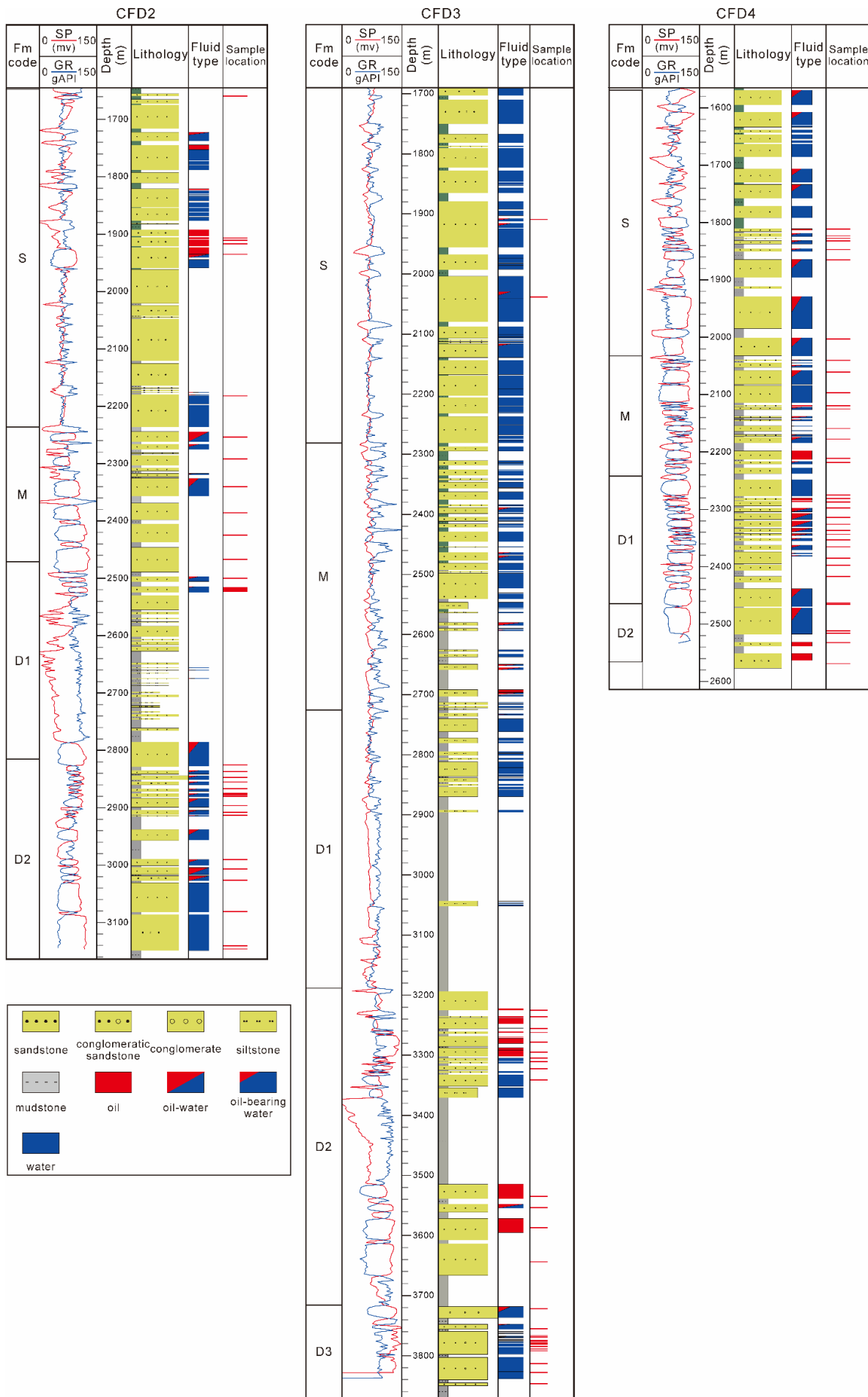


Figure S2. Lithology, logging, fluid type and sample locations in CFD2, 3 and 4. GR – gamma ray; SP –

spontaneous potential.

3. Error of laser grain size and the difference with thin-section grain size

We conducted repeated laser grain size experiments. The results show that the differences are very small. Here, we show an example (CFD4, 1811.5 m; Figure S3). The calculated sorting coefficients are 2.176 and 2.196, respectively. Therefore, the error is smaller than 1%.

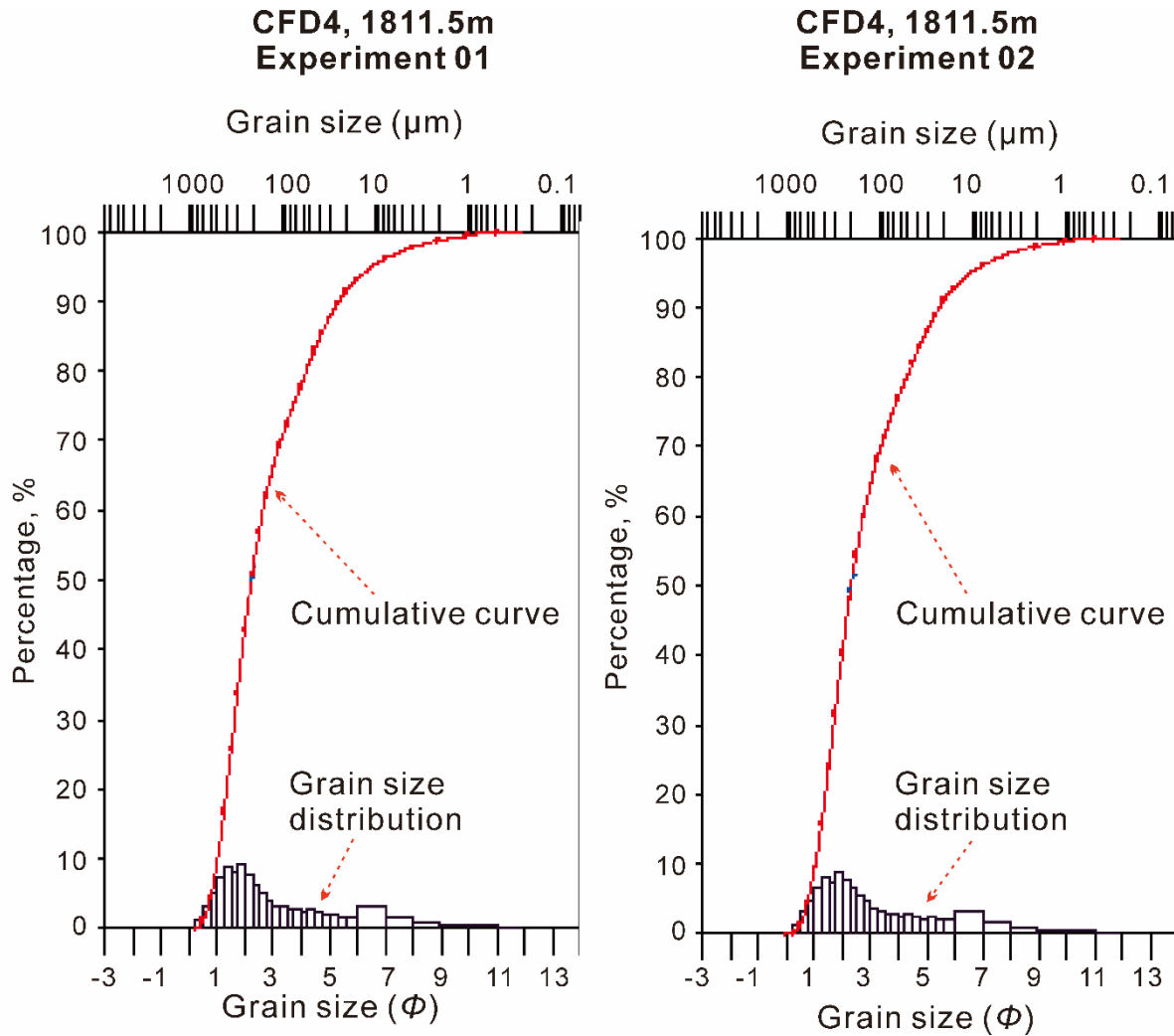
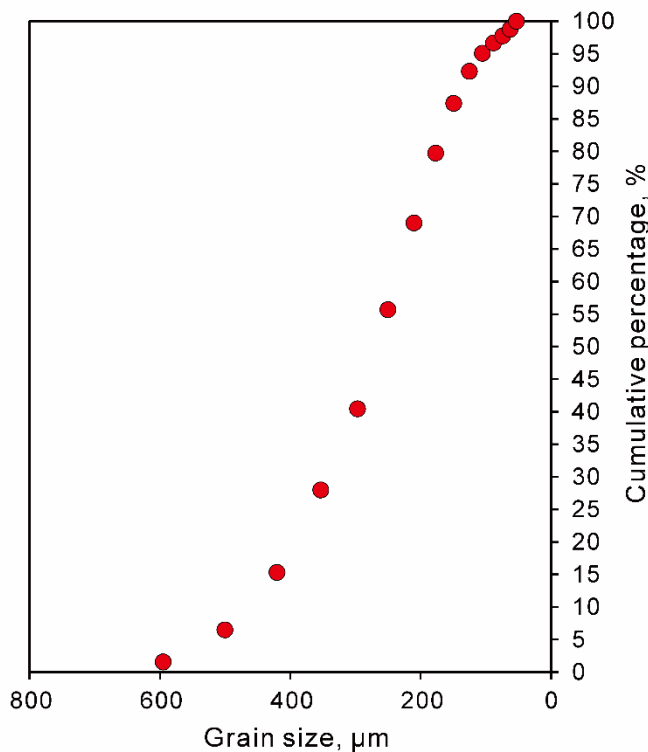


Figure S3. Repeated laser grain size experiments.

We measured the thin section grain sizes and compared the thin section grain size with laser grain size. Here, we show an example from CFD2, 2518.06 m. The results show that the method of thin section grain size underestimates the proportion of extremely fine grain size ($< 50 \mu\text{m}$; equivalent to $\Phi > 4.32$; Figure S4). The calculated sorting coefficients are 1.73 (laser grain size) and 1.86 (thin-section grain size), respectively. The difference of derived sorting coefficients between the two methods is 7.5%. We also measured other three samples (Table S1). The differences of derived sorting coefficients between the two methods are consistently smaller than 12%.

CFD2, 2518.06m
Thin section grain size



CFD2, 2518.06m
Laser grain size

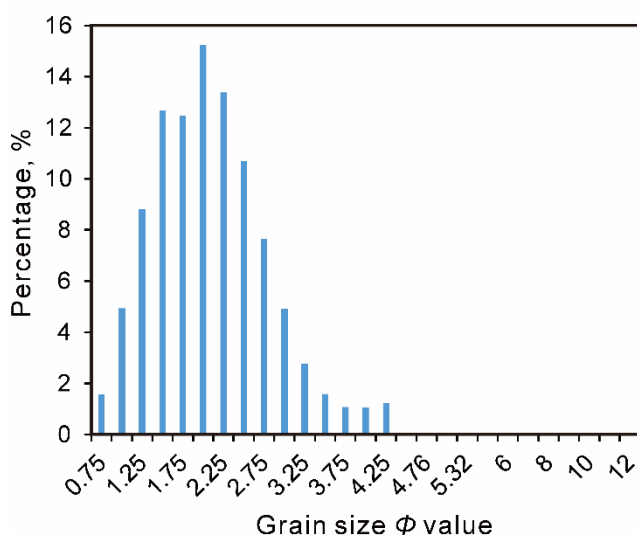
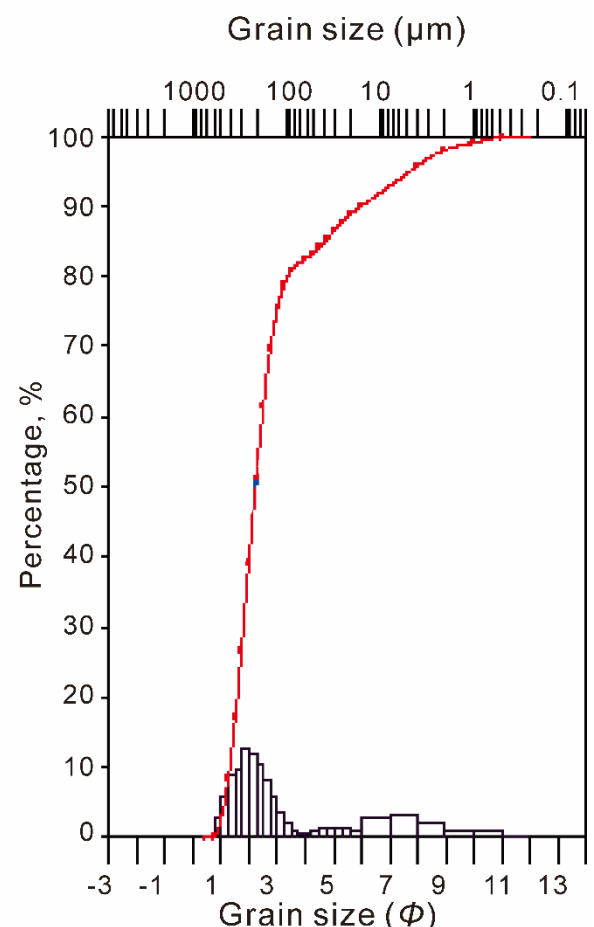


Figure S4. The difference between thin section grain size and laser grain size.

Table S1. Difference of derived sorting coefficient between thin section grain size and laser grain size.

Sample	Sorting coefficient		Difference/%
	Thin section grain size	Laser grain size	
CFD2, 2518.06 m	1.87	1.73	7.5%
CFD2, 2516.75 m	1.81	1.66	9.0%
CFD6, 1855 m	2.01	2.24	11.4%
CFD4, 2040.3 m	2.15	2.37	5.6%

4. Helium porosity and total thin section porosity

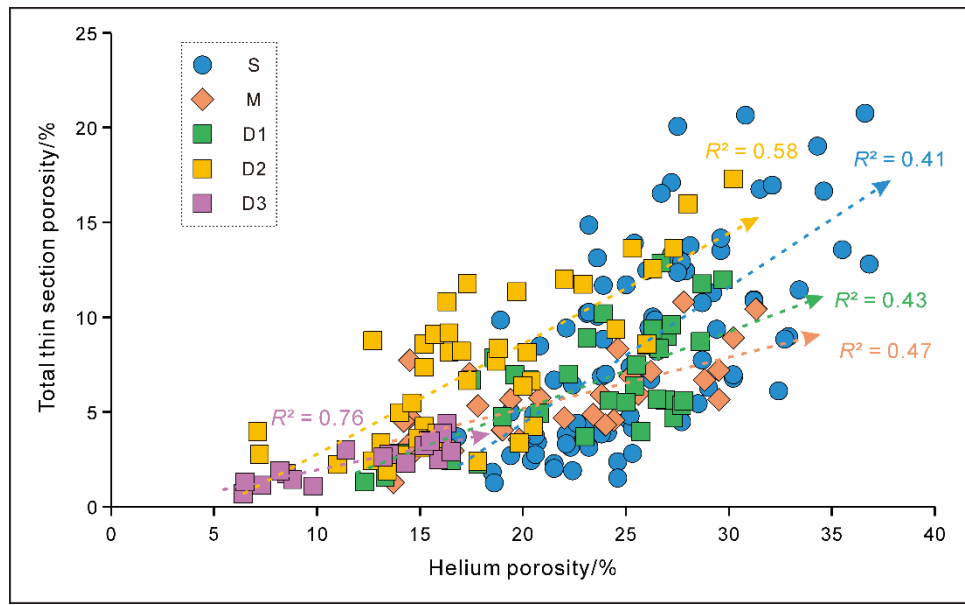


Figure S5. Correlations between helium porosity and total thin section porosity.

5. Controls of fault movement and fault surface geometry on fluid flow and seal

5.1 Geometry of fault surface

The seismic interpretation was conducted using 3-D seismic data. Based on the interpretation of the boundary fault in 2-D seismic profiles, the built-in function, fault contour of the GeoFrame was employed to generate the fault surface. The concave-convex geometry of the depth contour line of the fault surface resulted from different slope gradients along the fault strike. Central zones covering CFD9, CFD4, CFD10, CFD2, CFD6 and CFD1 exhibited considerably lower slope gradients than both flank zones (zone covering CFD7 and zone covering CFD5) (Figure S6). These results indicated that the fault surface was convex in the central zone and concave in both flank zones.

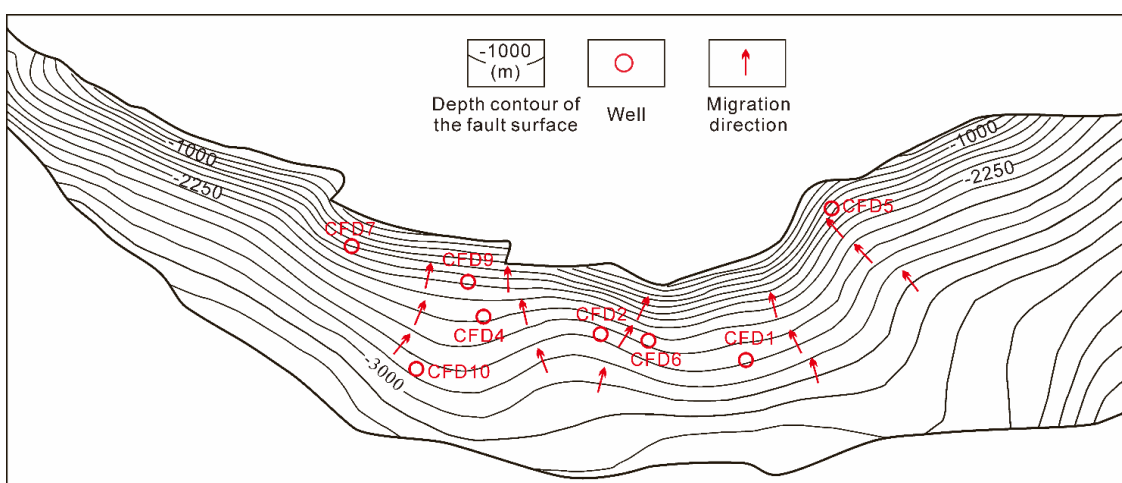


Figure S6. Depth contour line map of the boundary fault surface in the Caofeidian (CFD) area, indicating the

concave-convex geometry of the depth contour line of the fault surface and possibly preferable migration pathways for hydrocarbons and pore water.

5.2 Control of fault movement on fluid flow

Overall, the accumulation amount and the ‘accumulation+leakage’ amount show positive correlations with the Pliocene (A1) fault displacement rate (except at CFD1 and CFD7) (Figure S7). This indicates that the Pliocene (A1) fault movement activates the fluid migration.

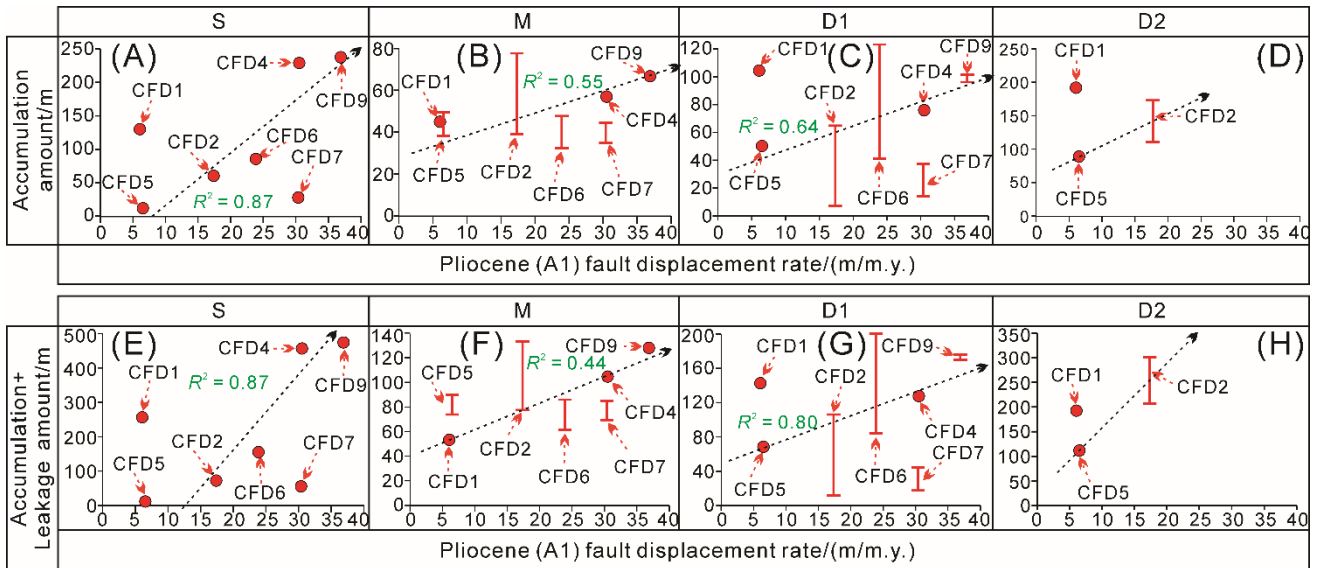


Figure S7. Correlations among the fault displacement rate and the accumulation amount and ‘accumulation+leakage’ amount of each stratum. The averaged values of accumulation and ‘accumulation+leakage’ amounts ranges were employed to calculate R^2 . The CFD1 and CFD7 data were not included when calculating R^2 .

CFD1 shows a unique accumulation characteristic. The Pliocene (A1) fault displacement rate at CFD1 is much lower than those at CFD6 and CFD2 (Figure 13). Therefore, theoretically, the hydrocarbon-show column height cannot be higher than that of CFD6 and CFD2 if the fluid was injected predominantly through faults. Therefore, it is reasonable to assume that the hydrocarbon accumulation in CFD1 mainly ran through internal lateral sandstones. Additionally, the low fault displacement rate at CFD1 led to the excellent sealing capability of faults, causing the oil to be well preserved. Thus, the hydrocarbon-show column height (oil leakage) at CFD1 is very small.

Although the Pliocene (A1) fault displacement rate at CFD7 is close to those of CFD9 and CFD4 (Figure 13), the hydrocarbon-show column height of every stratum in CFD7 is consistently less than those of CFD9

and CFD4 (Figure 14A, B, C). Hindle (1997) proposed that the fault plane geometry had an important influence on the vertical hydrocarbon migration pathway. The planar fault surface shape does not influence the concentration and dispersion of hydrocarbons, and the concave fault surface shape disperses hydrocarbons. Only convex fault surface shapes can concentrate hydrocarbons at the ridge zone of the convex, and therefore are beneficial for vertical hydrocarbon migration. The depth contour line map of the fault surface indicates that CFD7 does not lie in the convex zone (Figure S6). This result might indicate that CFD7 does not lie in the preferable migration direction of fluid, leading to the relatively weak accumulation at CFD7.

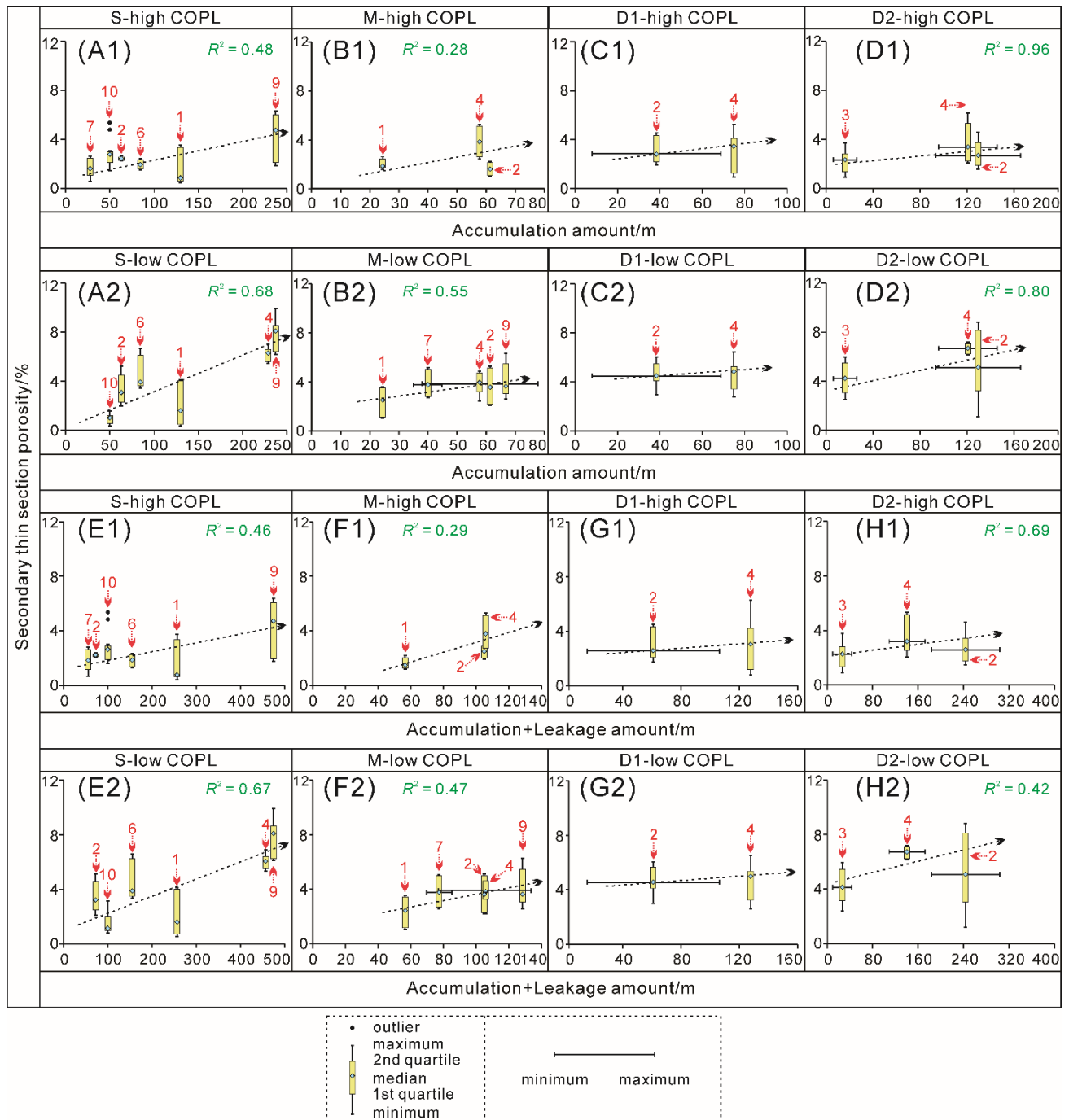


Figure S8. Correlations among the accumulation amount, ‘accumulation+leakage’ amount and secondary thin section porosity in each stratum. The inserted red numbers represent the boreholes. R^2 was derived using the

median secondary porosity values and averaged accumulation and ‘accumulation+leakage’ amounts. COPL - compactional porosity loss.

5.3 Evaluation of fault seal

5.3.1 Method for the evaluation of fault seal

Faults can act not only as conduits for fluid flow but also as seals. The mechanisms that lead to a fault acting as a seal could be juxtaposition, clay smear, cataclasis and diagenesis (e.g., calcite veins) (Knipe, 1992; Yielding et al., 1997; Vrolijk et al., 2016). Analysis of cataclasis and diagenesis requires direct observation and descriptive data of the fault zone, which is lacking in the study area. As an applicable way to estimate fault transmissibility, clay smears have been of interest in many studies in the context of sandstone/mudstone sequences. Scholars have proposed several methods to estimate clay smears, including the clay smear potential (*CSP*; Bouvier et al., 1989; Fulljames et al., 1997), shale smear factor (*SSF*; Lindsay et al., 1992) and shale gouge ratio (*SGR*; Eq. 2; Yielding et al., 1997; Freeman et al., 1998; Harris et al., 2002). The application of *CSP* and *SSF* requires detailed mapping of the thickness and offset of individual mudstone beds (Yielding et al., 1997). Therefore, this work employed the *SGR* calculation, which requires only the bulk fraction of mudstones in a stratum, to evaluate the fault seal capability (Figure 4; Yielding et al., 1997; Freeman et al., 1998).

$$SGR = \frac{\text{Zone thickness} \times \text{zone clay fraction}}{\text{directly measured fault vertical displacement}} \times 100\% \quad (2)$$

where the zone thickness was a window with a height equal to the directly measured fault vertical displacement and the clay fraction was derived from lithological data in the borehole.

In addition, some scholars have proposed using the across-fault pressure difference to calibrate the *SGR* (e.g., Bretan et al., 2003). However, all available boreholes used in this work lie in the hanging wall with respect to the boundary fault (Figure 1C). Therefore, we did not calibrate the *SGR* using pressure data.

5.3.2 Discussion of fault seal on fluid flow

Faults can act as transmissibility barriers in reservoirs and impede fluid flow (Harris et al., 2002). In sandstone/mudstone sequences, clay smears are considered an important mechanism related to the fault seal capability (Bouvier et al., 1989; Lindsay et al., 1992; Yielding et al., 1997; Freeman et al., 1998; Harris et al.,

2002; Vrolijk et al., 2016). For example, Yielding et al. (1997) proposed that an *SGR* value of 20% could be used as a threshold between no seal and seal.

There were no data on the oil column height and accumulation amount in the Upper Miocene (A2) and Pliocene (A1). Therefore, this work mainly discussed the correlations between the *SGR* of the Lower Miocene (S) fault and the oil column height and accumulation amount at S (Table S2). The calculation results showed that the *SGR* showed a positive relationship with the accumulation amount ($R^2 = 0.51$; Figure S9A). As the QGF and QGF-E indicated that present-day oil-bearing water and oil-water columns were all paleo-oil columns, the accumulation amount defined in this work represents paleo-oil accumulation amount. Therefore, this indicated that the clay smear in the fault zone well sealed paleo-oil columns. However, the *SGR* did not show relationship with present-day oil column height ($R^2 = 0.05$; Figure S9B). Fault displacement rate showed a positive relationship with the ‘accumulation+leakage’ amount ($R^2 = 0.87$; Figure S7E). This indicated that subsequent fault reactivation leads to the leakage of paleo-oil, leading some paleo-oil columns to be present-day oil-bearing water and oil-water columns. Therefore, fault reactivation might lead to the absence of relationship between *SGR* and present-day oil column height.

Table S2. *SGR* of the Lower Miocene (S) fault.

Borehole	<i>SGR</i> (%)
CFD7	31.01
CFD9	37.22
CFD4	22.25
CFD2	20.42
CFD6	8.70
CFD1	38.20
CFD5	3.10

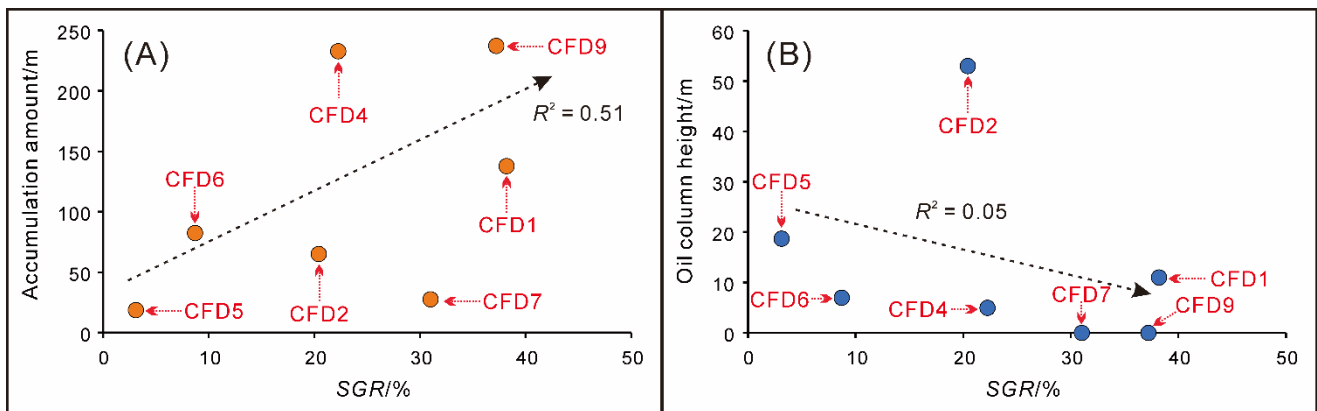


Figure S9. Correlations among *SGR* (Lower Miocene fault) and the accumulation amount and oil column

height at S. The data of CFD7 was not included when calculate R^2 .

The continuous existence of shale gouges depends on multiple conditions, including the shale contents, number and thickness of slipped shale beds, fault core structures, and in situ stresses (Vrolijk et al., 2016). Vrolijk et al. (2016) summarized the evolution and growth process of clay smears, which could be subdivided into (1) the shale incorporation process, (2) the clay smear evolutionary process and (3) clay smears in over-consolidated rocks. This growth process might lead to a change in the seal efficiency of clay smears. Moreover, clay smears might incorporate sands and gravels (e.g., Heynekamp et al., 1999), which also changes the seal capability of clay smears. Furthermore, even if a continuous clay smear exists in the fault core, secondary fractures might cut clay smears and therefore provide conduits for fluid flow. Secondary fractures in the fault core crossing clay smears have been found in many outcrops (e.g., van der Zee et al., 2003; Vrolijk et al., 2016). Therefore, during the reactivation process of the fault, the fault zone would experience a process from open (high permeability) to seal (low permeability) (Hooper, 1991; Cox et al., 1995; Boles et al., 2004; Zhang et al., 2010; Mozafari et al., 2015, 2017). Therefore, it was reasonable that subsequent fault reactivation destroyed the seal efficiency of clay smears, leading to the leakage of hydrocarbons. Cases of the fluid leakage through faults have also been found in other areas, e.g., hydrocarbon leakage in the Fulmar Formation, North Sea, UK (Wilkinson et al., 2006), the Orange Basin, South Africa (Isiaka et al., 2017) and the Hammerfest Basin, Southwestern Barents Sea (Mohammedyasin et al., 2016); and CO₂ leakage in the Paradox Basin, southeastern Utah (Naruk et al., 2019) and the Colorado Plateau, east-central Utah (Jung et al., 2014).

6. Correlations between COPL, CEPL, and total secondary thin section porosity

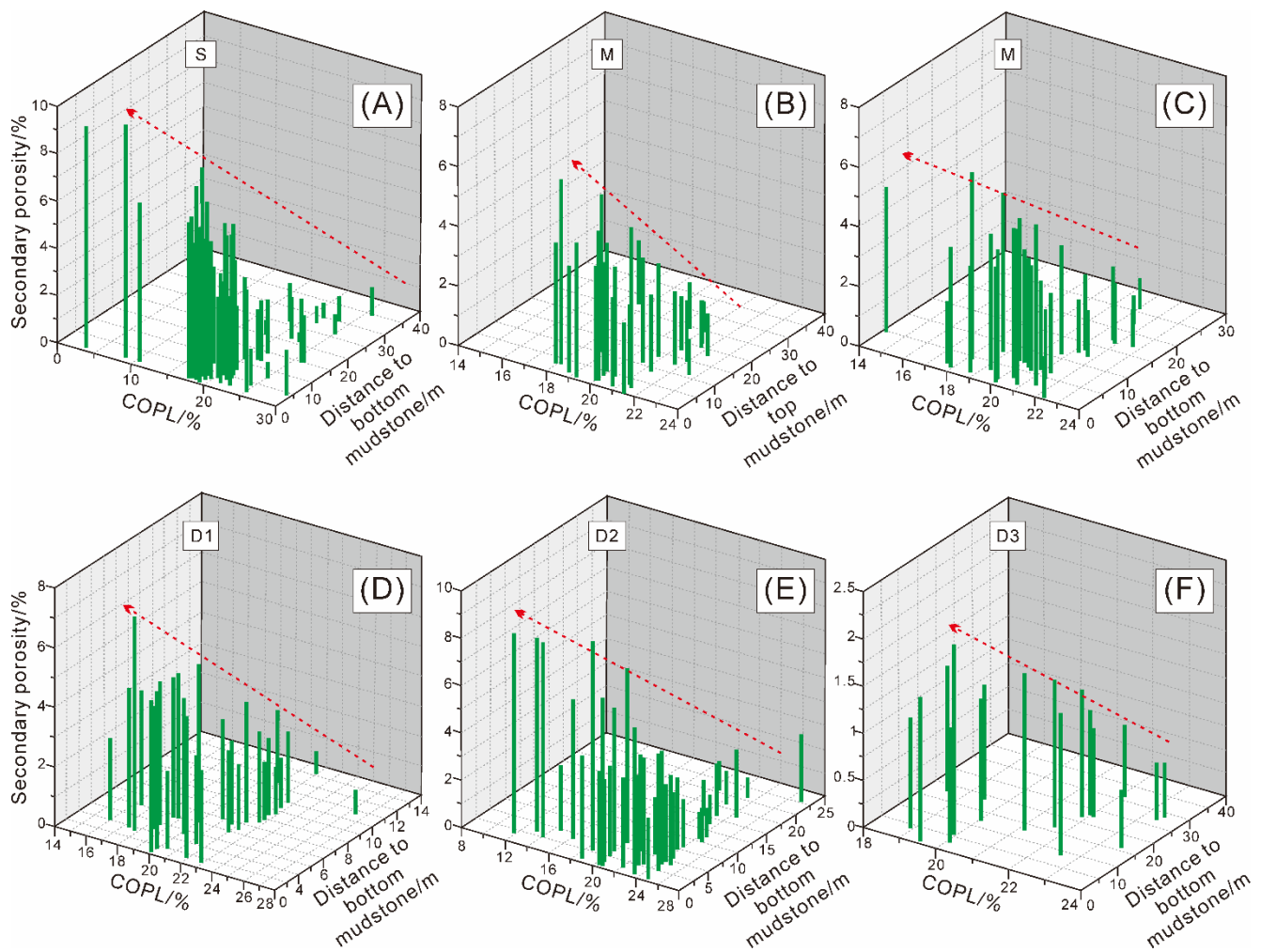


Figure S10. 3-D bar charts showing the distribution of secondary porosity in each stratum with relationships to both the compactional porosity loss (COPL) and the distance to the sandstone/mudstone boundary. CEPL – cementation porosity loss.

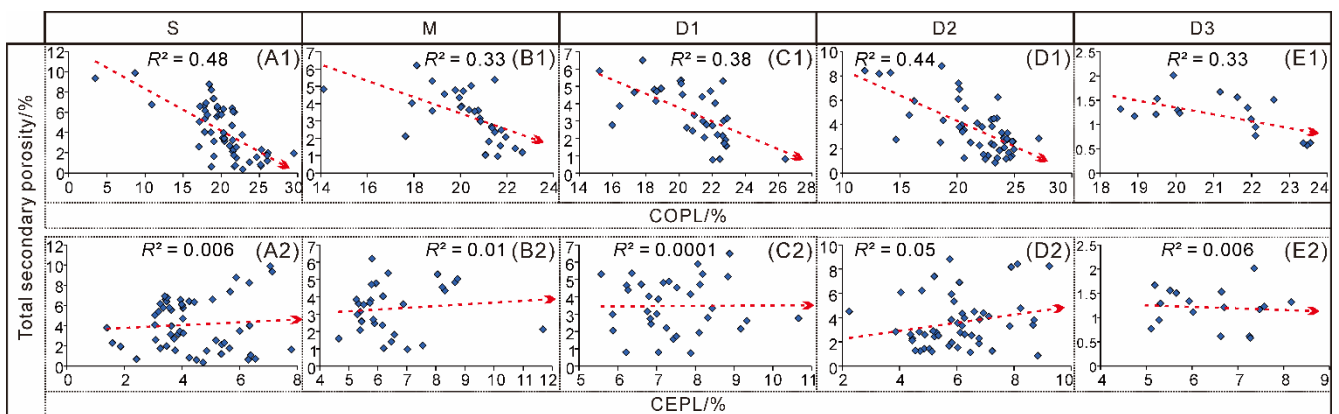


Figure S11. Correlations among compactional porosity loss (COPL), cementation porosity loss (CEPL), and total secondary thin section porosity at each stratum. COPL consistently shows negative correlations with total secondary thin section porosity at each stratum. However, CEPL shows absence of correlations with total

secondary thin section porosity at each stratum.

References

- Bouvier, J. D., C. H. Kaars-Sijpesteijn, D. F. Kluesner, C. C. Onyejekwe, and R. C. van der Pal, 1989, Three-dimensional seismic interpretation and fault sealing investigations, Nun River Field, Nigeria: American Association of Petroleum Geologists Bulletin, v. 73, no. 11, p. 1397–1414, doi: 10.1306/44B4AA5A-170A-11D7-8645000102C1865D.
- Bretan, P., G. Yielding, and H. Jones, 2003, Using calibrated shale gouge ratio to estimate hydrocarbon column heights: American Association of Petroleum Geologists Bulletin, v. 87, no. 3, p. 397–413, doi: 10.1306/08010201128.
- Ehrenberg, S. N., 1989, Assessing the relative importance of compaction processes and cementation to reduction of porosity in sandstones: discussion; compaction and porosity evolution of Pliocene sandstones, Ventura Basin, California: discussion: American Association of Petroleum Geologists Bulletin, v. 73, no. 10, p. 1274–1276, doi: 10.1306/44B4AA1E-170A-11D7-8645000102C1865D.
- Freeman, B., G. Yielding, D. T. Needham, and M. E. Badley, 1998, Fault seal prediction: the gouge ratio method: Geological Society, London, Special Publications, v. 127, p. 19–25, doi: 10.1144/GSL.SP.1998.127.01.03.
- Fulljames, J. R., L. J. J. Zijerveld, and R. C. M. W. Franssen, 1997, Fault seal processes: systematic analysis of fault seals over geological and production time scales, in P. Møller-Pedersen, and A. G. Koestler, eds., Hydrocarbon seals: Importance for exploration and production: Norwegian Petroleum Society Special Publication, p. 51-59, doi: 10.1016/S0928-8937(97)80006-9.
- Harris, D., G. Yielding, P. Levine, G. Maxwell, P. T. Rose, and P. Nell, 2002, Using shale gouge ratio (SGR) to model faults as transmissibility barriers in reservoirs: an example from the Strathspay field, North Sea: Petroleum Geoscience, v. 8, p. 167–176, doi: 10.1144/petgeo.8.2.167.
- Heynekamp, M. R., L. B. Goodwin, P. S. Mozley, and W. C. Haneberg, 1999, Controls on fault-zone architecture in poorly lithified sediments, Rio Grande Rift, New Mexico: implications for fault-zone permeability and fluid flow, in W. C. Haneberg, P. S. Mozley, J. C. Moore, and L. B. Goodwin, eds., Faults and subsurface fluid flow in the shallow crust: American Geophysical Union, p. 27–49, doi:

10.1029/GM113p0027.

- Isiaka, A. I., R. J. Durrheim, M. S. D. Manzi, and M. A. G. Andreoli, 2017, 3D seismic analysis of the AK Fault, Orange Basin, South Africa: Implications for hydrocarbon leakage and offshore neotectonics: *Tectonophysics*, v. 721, p. 477–490, doi: 10.1016/j.tecto.2017.10.011.
- Knipe, R. J., 1992, Faulting processes and fault seal, *in* R. M. Larsen, H. Brekke, B. T. Larsen, and E. Talleras, eds., Structural and tectonic modelling and its application to petroleum geology: Norwegian Petroleum Society Special Publications, p. 325–342, doi: 10.1016/B978-0-444-88607-1.50027-9.
- Lander, R. H., and O. Walderhaug, 1999, Predicting porosity through simulating sandstone compaction and quartz cementation: *American Association of Petroleum Geologists Bulletin*, v. 83, no. 3, p. 433–449, doi: 10.1306/00AA9BC4-1730-11D7-8645000102C1865D.
- Lindsay, N. G., F. C. Murphy, J. J. Walsh, and J. Watterson, 1992, Outcrop studies of shale smears on fault surface, *in* S. S. Flint, and I. D. Bryant, eds., The geological modelling of hydrocarbon reservoirs and outcrop analogues: International Association of Sedimentologists Special Publication 15, p. 113–123, doi: 10.1002/9781444303957.ch6.
- Lundegard, P. D., 1992, Sandstone porosity loss – A “big picture” view of the importance of compaction: *Journal of Sedimentary Petrology*, v. 62, no. 2., p. 250–260, doi: 10.1306/D42678D4-2B26-11D7-8648000102C1865D.
- Mohammedyasin, S. M., S. J. Lippard, K. O. Omosanya, S. E. Johansen, and D. Harishidayat, 2016, Deep-seated faults and hydrocarbon leakage in the Snøhvit Gas Field, Hammerfest Basin, Southwestern Barents Sea: *Marine and Petroleum Geology*, v. 77, p. 160–178, doi: 10.1016/j.marpetgeo.2016.06.011.
- Taylor, T. R., M. R. Giles, L. A. Hathon, T. N. Diggs, N. R. Braunsdorf, G. V. Birbiglia, M. G. Kittridge, C. I. Macaulay, and I. S. Espejo, 2010, Sandstone diagenesis and reservoir quality prediction: Models, myths, and reality: *American Association of Petroleum Geologists Bulletin*, v. 94, no. 8, p. 1093–1132, doi: 10.1306/04211009123.
- van der Zee, W., J. L. Urai, and P. D. Richard, 2003, Lateral clay injection into normal faults: *GeoArabia*, v. 8, no.3, p. 501–522, doi: 10.2113/geoarabia0803501.
- Vrolijk, P. J., J. L. Urai, and M. Kettermann, 2016, Clay smear: Review of mechanisms and applications: *Journal of Structural Geology*, v. 86, p. 95–152, doi: 10.1016/j.jsg.2015.09.006.

Yielding, G., B. Freeman, and D. T. Needham, 1997, Quantitative fault seal prediction: American Association of Petroleum Geologists Bulletin, v. 81, no. 6, p. 897–917, doi: 10.1306/522B498D-1727-11D7-8645000102C1865D.